ELSEVIER

Journal of Power Sources 80 (1999) 134–141

JOURNAL OF POWER SOURCES

Electrochemical efficiency in multiple discharge/recharge cycling of supercapacitors in hybrid EV applications

Wendy G. Pell [a], Brian E. Conway [a,*], William A. Adams [b], Julio de Oliveira [b]

[a] *Chemistry Department, University of Ottawa, 10 Marie Curie Street, Ottawa, Ontario, Canada, K1N 6N5*
[b] *ESTCO and IEA Electric Hybrid Vehicle Operating Agency (Annex 5), Nepean, Ontario, Canada*

Abstract

The use of large capacitance supercapacitors in series or series/parallel configurations has been envisaged and evaluated as a basis for load-levelling, and hence performance enhancement, in electric vehicles (EV) powered primarily by rechargeable batteries or fuel-cells. In this paper, charge/discharge efficiency in duty-cycles of the supercapacitor component are examined in relation to distributed resistance in porous double-layer and redox-type devices which restricts efficiency of discharge and recharge cycling, especially at high rates. Results of quantitative experiments on the responses of a five-element RC model hardware equivalent-circuit and a gold brush electrode are presented. Potential-recovery after discharge and potential-decay after recharge, and potential changes following load variations, enable efficiencies of charge delivery and acceptance to be evaluated.

Keywords: Supercapacitors; Porous electrodes; Hardware simulation

1. Introduction

1.1. Sources of inefficiency in electrochemical systems

Efficiency of energy delivery and storage is an important factor in design of power-trains for hybrid EV systems. Identification and understanding of sources of inefficiency in both the areas of rechargeable battery technology and in the development and operation of electrochemical supercapacitors are essential requirements for optimization of such systems.

In theory, an electrochemical energy source can provide complete utilization of the Gibbs free energy of the chemical oxidation/reduction processes involved in the overall cell reaction, but only if it is conducted reversibly at zero or low overvoltage, η.

The overvoltage at practical current-densities, i, is resolvable into three components as follows: (a) the intrinsic, kinetic or 'activation' polarization, η_a, associated with slowness of the electrode processes involved, inherent in any electrode reaction rate process, is a logarithmic function of i or I; (b) Ohmic polarization, η_0, or 'IR'-drop effects due to passage of finite current, I, dependent on the solution conductivity and the electrode area, is a linear function of I; and (c) concentration polarization, η_c, due to build up of a concentration-gradient at a working electrode surface caused by consumption of the reactant. Overall, the polarization, η, is the sum of η_a, η_0 and η_c.

1.2. Energy losses in the charging and discharging of electrochemical capacitors

Normally, no regular faradaic currents pass during charging or discharging of double-layer (e.g., high-area carbon) capacitors if they are 'ideally polarizable' (Grahame, [1]). However, up to about 5% of charging/discharging currents, and corresponding integrated charges, can be due to faradaic reactions at the carbon interface involving oxidation/reduction of reactive surface-oxide functionalities [2]. Such currents can then be associated with activation polarization, η_a and depend very much on the provenance and pretreatment [2,3] of the high-area carbon material.

More direct η_a polarization can arise in the case of pseudocapacitance, C_Φ, [4,5] associated with redox processes at high-area oxide films, e.g., RuO_2, Co_3O_4, IrO_2, Mo_xN etc. [6,7] as pseudocapacitance is usually associated with passage of faradaic currents required to effect the conversion $Ox + ze \Leftrightarrow Red$. Pseudocapacitance, for such systems, is generally some ten times that of the double-layer.

Any involvement of significant η values in electrochemical capacitor charge/discharge processes corre-

* Corresponding author. Tel.: +1-613-562-5728; Fax: +1-613-562-5170

0378-7753/99/$ - see front matter
PII: S0378-7753(98)00257-2

sponds to irreversible dissipation of energy, G, determined by:

$$G = \frac{1}{2}q(\eta) \quad \text{or} \quad \frac{1}{2}C(\eta)^2. \tag{1}$$

As discussed elsewhere [8], the η effects are the principal reasons for declining energy- and power-densities with increase of charging or discharging rates, characterized by Ragone plots [9] of power-density vs. energy-density (or logs thereof).

Two aspects of efficiency in battery or capacitor cycling will be briefly discussed.

(a) Current efficiency is the percentage extent (ideally 100) to which charge is delivered or taken up by the desired electrochemical or electrical processes in relation to that passed in side-reactions. With electrochemical capacitors, the latter rarely require consideration except in the event of overcharge (or overdischarge) which can impair performance in ongoing cycling and/or lead to excessive self-discharge.

(b) Energy storage efficiency, ε, on charge or discharge is one of the main concerns in operation of electrochemical capacitors, especially in high-rate applications. For a pure capacitor, having zero real or equivalent series resistance, the efficiency of charge (energy) acceptance or delivery is 100%. However, in a configuration having a real or equivalent series resistance, R, irreversible dissipation of energy as I^2R loss takes place, leading to $\varepsilon < 100\%$.

1.3. Energy dissipation in a porous electrode

As emphasized in the work of de Levie [10] and in various later works [e.g., Refs. [11,12]], the essential difference between a porous electrode and a planar conducting one lies in the distribution of double-layer capacitance coupled in series-parallel ways with solution resistance (and sometimes significantly with the resistance of the matrix of the porous material). Thus, for a porous electrode the IR-drop and the ohmic dissipation of energy, I^2R, are no longer single-valued quantities at a given I, but vary down the pore: the local I diminishes and the cumulative R increases due to a *continuous* increase of electrolytic resistance down the pore from its orifice. Consequently any charging (or discharging) signal does not have an immediate and uniform effect on the time-dependent state of charge (or discharge) of the device and no unique RC time-constant characterizes the response function for such an electrode subject to a.c., a.v. (alternating current/voltage) or pulse modulation and the impedance is substantially frequency dependent. In the case of a.v. modulation, there arises a 'penetration depth' [10] of the effect of the signal down the pore dependent on the conductivity and diameter of the pore, and the frequency of the a.v. signal. The resulting response is close to that of a transmission line R–C network which has a 45° phase angle between the real and imaginary components of its impedance as shown experimentally by de Levie for a 'brush electrode', simulating the behaviour of a matrix of parallel, linear pores [13]. At high frequencies, the C–R of only the outer orifice region of the pore is modulated so the measured capacitance becomes dispersed to that of only the projected outer surface area of the porous electrode.

Hence, for such a porous matrix configuration, the effective IR-drop increases at lower frequencies as the d.c. polarization limit is approached. Correspondingly, the local energy dissipation, 'I^2R', depends on frequency and the depth addressed down the pore. Thus, an integrated energy dissipation should be calculated in order to evaluate efficiency of charging as a function of rate.

The same situation arises for the response to a pulsed regime of charging/discharging current. There is a distribution of the extent of charging (or discharging) down the pore, and upon interruption of a pulsed charge (or discharge) there is an internal time-dependent redistribution of charge within the porous electrode until (on open-circuit) an equipotential is set up. After longer times, a continuing, overall, self-discharge usually takes place according to faradaic and/or diffusion-controlled processes that occur across the previously charged double-layer. The mechanisms and kinetic behaviours of such self-discharge processes were treated in detail in recent papers by Conway et al. [14] and by Liu et al. [15].

The internal redistribution of charge and associated currents cannot be accessed experimentally in a real porous electrode but the overall effects are observable in terms of a component of the self-discharge behaviour and of repetitive, time-dependent, voltage recovery studied by Conway et al. [14]. However, as in the present work, it is very informative to directly measure the redistribution effects by means of experimental examination using a series-parallel R–C hardware model of a porous-electrode pore.

2. Experimental

2.1. Nature of the model hardware circuit

Miller [12] recently showed, by computer-simulation, that the wide-band a.c. frequency-response of a selected real capacitor device (Panasonic or Evans type capacitors) could be well represented by that of a 5-element, series-parallel network of appropriately valued capacitors and resistors, and such a model hardware circuit was used in this work (Fig. 1). The distribution of component charging currents are indicated as I_a, I_b, I_c, I_d, and I_e passing, respectively, into C_a, $C_b \ldots C_c$. I_0 is the total charging (or discharging) current admitted between terminals WE and CE, and is equivalent to the sum of the components I_a to I_e. The currents passing, respectively, through each of R_1, $R_2 \ldots R_4$, down the 'pore', are I_1, $I_2 \ldots I_4$. The five capacitors have capacitance values in the range of 130 to 142 μF and the resistors are approximately 100 kΩ.

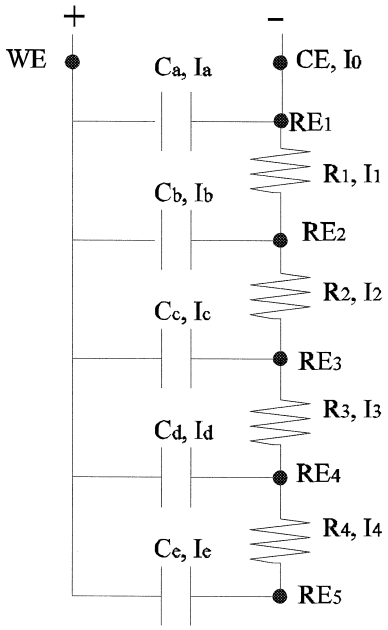

Fig. 1. Hardware model circuit for evaluation of efficiency aspects of charge and discharge cycling at a single pore in a porous capacitor electrode. The constant current signal was applied across terminals WE and CE, while the voltage response to this signal was measured across terminals WE and RE_n, ($n = 1, 2, \ldots, 5$).

2.2. Experimental procedure

Prior to each experiment, all capacitors in the network were fully discharged (to 0 V), so that the initial open-circuit voltage was 0 V. In each case, 10 to 15 constant-current charges/discharges of 50, 100 and 200 μA, were applied sequentially between 0 and 9 V across the CE and WE terminals of the network. The recorded voltages were measured between the 5 'reference' points (RE_1, $RE_2, \ldots RE_5$) and WE corresponding to potential differences V_a to V_e down the hardware circuit (Fig. 1). Cyclic voltammograms were also obtained at various sweep rates in the usual way. A 60 strand gold wire brush electrode (60 mm in length, 0.2 mm in diameter) as described by de Levie [13] was also studied in 0.02 and 0.2 M H_2SO_4. CV and self-discharge experiments were conducted within the potential range 0.1 to 1.1 V (RHE), i.e., the double-layer charging region.

3. Results

3.1. Charge / discharge voltage and current behaviour

Fig. 2 shows the 100 μA charge/discharge voltage vs. time profiles, and Fig. 3 the corresponding local component current vs. time profiles, of the first two cycles addressed to the network. Curves $V_a \ldots V_e$ (and $I_a \ldots I_e$, respectively) show the separate profiles down the 'pore'

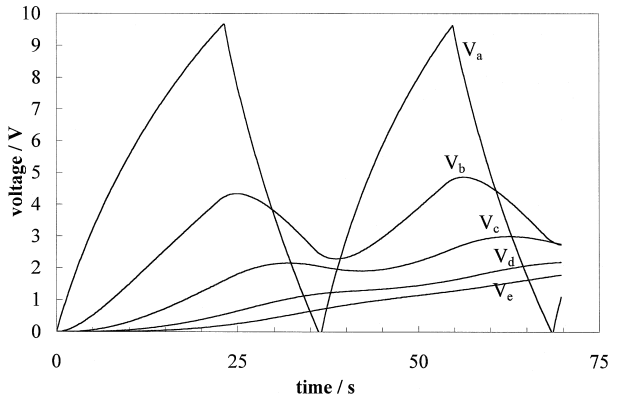

Fig. 2. Voltage vs. time profiles of the first and second cycles addressed to the network, resolved for each of the capacitors shown in Fig. 1. $I_0 = 100$ μA. Curves V_a, $V_b \ldots V_e$ show the separate profiles across each of the five capacitors C_a, $C_b \ldots C_e$.

circuit at the five reference points indicated in Fig. 1. Note the differences of the first and second cycle curves that arise due to the 'memory effect' associated with the distribution of charging/discharging times within the complex *R–C* circuit. Figs. 4 and 5 show the circuit-element behaviours on the 11th and 12th cycles where a more or less 'steady-state' in the discharge/recharge processes has been reached. Note that attenuation of responses down the 'pore' for potentials V_a to V_e and currents I_a to I_e, and the phase-shift between these V and I vs. t profiles, are already noticeable in Figs. 2 and 3.

A significant feature of the charging and succeeding discharge curves (Figs. 2 and 4), unlike charging/discharging of a regular plane-electrode capacitor, is that they are not linear in time, even for the V_a potential, nor are they mirror-images, thus demonstrating one of the essential features of the electrical behaviour of porous electrode capacitors. A linear charge/discharge curve is expected for a capacitor (of constant capacitance) charged at constant current. This is not the case for the *R–C* network

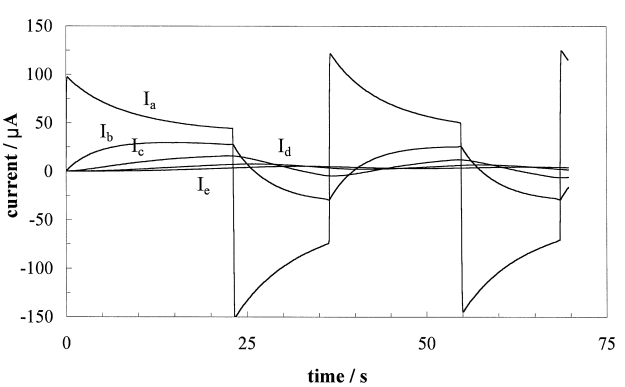

Fig. 3. Current vs. time profiles of the 1st and 2nd cycles addressed to the network, resolved for each of the capacitors shown in Fig. 1. $I_0 = 100$ μA. Curves I_a, $I_b \ldots I_e$ show the separate profiles of currents passing, respectively, into each of the five capacitors C_a, $C_b \ldots C_e$.

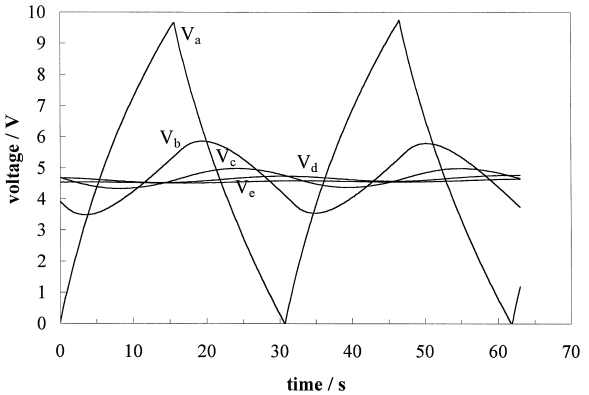

Fig. 4. Voltage vs. time profiles of the 11th and 12th cycles addressed to the network, resolved for each of the capacitors shown in Fig. 1. $I_0 = 100$ μA. Curves V_a, $V_b \ldots V_e$, show the separate profiles across each of the five capacitors C_a, $C_b \ldots C_e$.

used in this study; while the total current, I_0, supplied to the network is constant, the current admitted or delivered by each capacitor is not—the result being a voltage response that is non-linear in time (Figs. 3 and 5). This distortion becomes characteristically much more significant for the charge/discharge curves further down the 'pore', i.e., for potentials V_b, V_c, V_d and V_e as a function of time (Figs. 2 and 3), and the differences between the first-cycle and second-cycle charge/discharge curves become much increased as V goes from V_b to V_e (down the pore), with more and more asymmetry. Note that this aspect of their behaviour would become attenuated for smaller values of R_1 to R_4; obviously, in the limit of R_1, $R_2 \ldots R_4 \rightarrow 0$, the circuit becomes simply that of five capacitors directly in parallel for which the overall C is given by:

$$C_{\text{overall}} = \sum_{n=1}^{n=5} C_n.$$

Interestingly, as I_a is decreasing because of charging of capacitor C_a, I_b, $I_c \ldots$ etc. are increasing; corresponding differences in t-dependence arise in the discharge current profiles. Note that the second-cycle profiles are not, respectively, identical to the first-cycle ones. However, by the 11th and 12th cycles, a 'steady-state' has been set up and the successive component-current profiles are almost identical in their time-dependence (Fig. 5). Comparison of these figures results in several interesting and significant observations. Firstly, in the early cycles, the current to these inner capacitors is generally positive (i.e., the inner capacitors are continuously being charged even while the outer capacitors discharge). By the 11th and 12th cycles, however, the inner capacitors begin to experience both charge and discharge in the time period required to fully charge and discharge the outermost capacitor, C_a. Secondly, the currents passing to the capacitors after 11 or 12 cycles are smaller than those initially experienced. Thirdly, the shape of the current/time profile changes, especially in the case of I_c (see Figs. 4 and 5). With time, the current profile becomes more sinusoidal in shape.

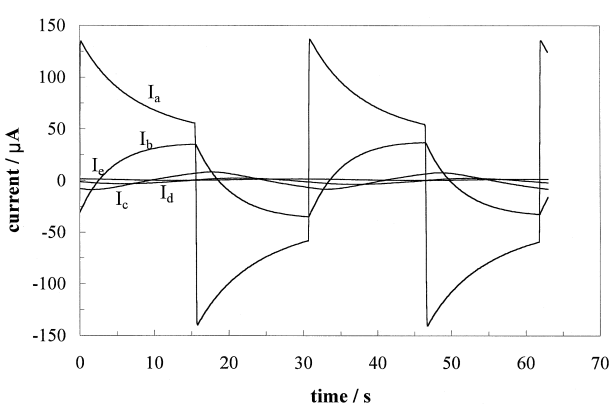

Fig. 5. Current vs. time profiles of the 11th and 12th cycles addressed to the network, resolved for each of the capacitors shown in Fig. 1. $I_0 = 100$ μA. Curves I_a, $I_b \ldots I_e$., show the separate profiles of currents passing, respectively, into each of the five capacitors C_a, $C_b \ldots C_e$.

The behaviours for first and second (and also 11th and 12th or 7th and 8th, respectively) cycles at 200 μA and 50 μA are qualitatively similar. At higher rate (and, therefore higher IR drop) the V_b, V_c, V_d and V_e profiles arise at lower voltages. The extent of cycling required before 'steady-state' is attained is also dependent on rate; at 50 μA fewer than 8 cycles are required, at 100 μA the inner capacitors have reached 'steady-state' after completion of 12 cycles, and at 200 μA after 12 cycles the three innermost capacitors are still experiencing a net charging current. Thus as the total I_0 increases, the inner capacitors charge relatively more slowly due to increased energy and power losses through the outer resistors. Further, at low rate, the 'amplitude of the voltage oscillation' experienced by the inner capacitors is greater.

3.2. Power, P, and energy, E, losses

One of the most significant aspects of the performance of supercapacitors is their capability of delivering power at high power-densities. In addition, the relation of the latter to energy-densities is of corresponding importance, as revealed by Ragone plots [9].

From the experimental data for component V and I behaviour, it is possible to calculate the power losses, P, down the pore-circuit as

$$P_n = \left[I_n(t) \right]^2 R_n \qquad \text{for } n = 1,2,3,4 \tag{2}$$

The current components on the first and second cycles, as well as 11th and 12th cycles, down the resistor elements R_1, $R_2 \ldots R_4$ were determined as a function of time. The currents through the resistors are generally higher for the first and second cycles as compared to the 11th and 12th. Further, during the first cycle, only the outermost resistor experiences a current flowing in both the 'charging' and 'discharging' directions. The inner resistors see only

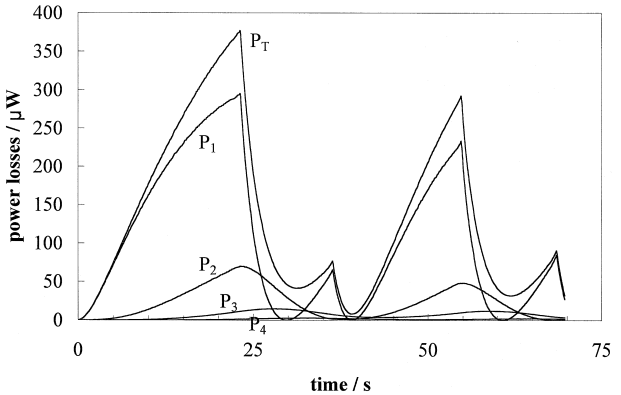

Fig. 6. Component dissipated power losses, P_1, $P_2, \ldots P_4$ through resistors R_1, $R_2, \ldots R_4$, respectively, together with the total power loss, P_T. $I_0 = 100$ μA for the 1st and 2nd cycles

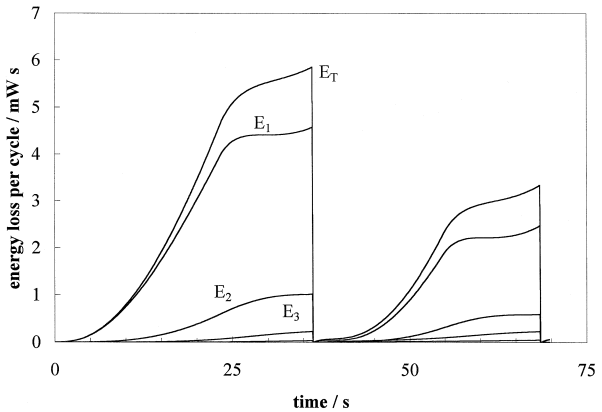

Fig. 8. Component dissipated energy losses per cycle, E_1, $E_2 \ldots E_4$ through resistors R_1, $R_2, \ldots R_4$, respectively, together with the total power loss, E_T. $I_0 = 100$ μA for the 1st and 2nd cycles.

'charging' currents. By the 11th and 12th cycles current passes in *both* directions through each of the resistors, and 'steady-state' I–t profiles have again been attained. Fig. 6 shows the resulting power loss behaviour for first and second cycles at 100 μA overall charge/discharge currents giving the component element power losses, P_1, P_2, P_3 and P_4, together with the total P (P_T). Note the unusual shapes of the curves and the difference of the second-cycle component P(time) curves from those for the first cycle. On the 11th and 12th cycles the component element power lines are shown in Fig. 7. Observe that now the P_1 curve is almost identical with the P_T curve while P_2, P_3 and P_4 (≈ 0) are much smaller for both charge and discharge half-cycles. The differences become exaggerated because the current components are squared for the calculation of values of P.

The corresponding energy losses can, of course, also be calculated and are:

$$E_n = \int_0^t \left[I_n(t) \right]^2 R_n dt \qquad \text{for } n = 1,2,3,4 \tag{3}$$

Fig. 8 shows plots of the total and component energy losses, E_T, $E_1 \ldots E_4$ vs. time for first and second cycles, corresponding to the respective $V(t)$ and $I(t)$ relations shown earlier. The second-cycle behaviour is quite different and the energy losses are much diminished. On the 11th and 12th cycles, a 'steady-state' is again almost reached (Fig. 9) and the two series of curves are almost identical. Note, as for the P curves, $E_1(t)$ is almost identical with $E_T(t)$, while E_2, E_3 and E_4 are practically zero. It is from the analysis of these integrated resistive losses that the energy storage efficiency, ε, may be calculated. For a 100 μA charge, once 'steady-state' has been reached, an energy storage efficiency during charge of approximately 85–86% was achieved.

Power losses are greater at 200 μA as compared with 100 or 50 μA for all cycles, while energy losses per cycle are highest at the 50 μA charge rate. Interestingly, at lower rates, the power losses through the inner resistive elements (R_2, R_3 and R_4) become significantly more important than at high rate where losses through R_1 account for more than 90% of the total power losses. These differences result because the power losses are dependent

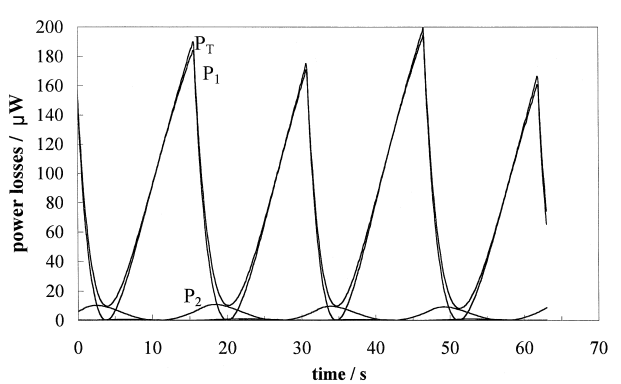

Fig. 7. Component dissipated power losses, P_1, $P_2, \ldots P_4$ through resistors R_1, $R_2, \ldots R_4$, respectively, together with the total power loss, P_T. $I_0 = 100$ μA for the 11th and 12th cycles.

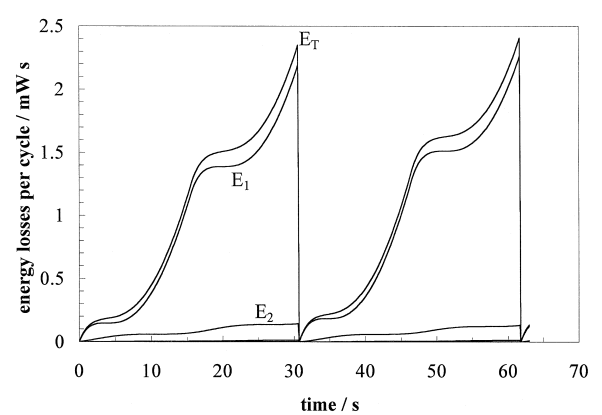

Fig. 9. Component dissipated energy losses per cycle, E_1, $E_2 \ldots E_4$ through resistors R_1, $R_2, \ldots R_4$, respectively, together with the total power loss, E_T. $I_0 = 100$ μA for the 11th and 12th cycles.

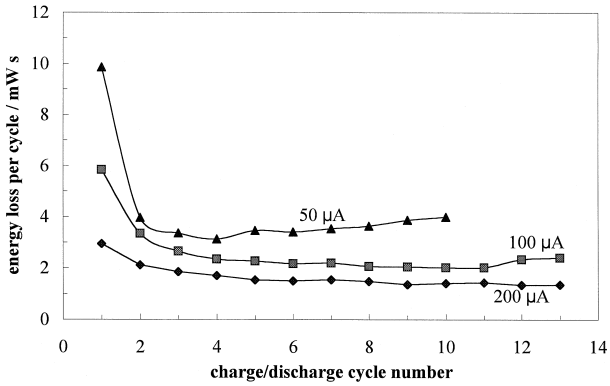

Fig. 10. Resistive energy losses for charging/discharging rates of 50, 100, and 200 μA as a function of cycle number.

on the magnitude of I^2, whereas the energy losses incorporate a time component.

It should be noted that while a significant increase in energy losses was found at the lower rate, an increase in the total energy stored and therefore, in the energy-density of the material or device, was also found. Also, we see at lower rates, that the losses through the inner resistive elements contribute significantly to the total energy loss, whereas at high-rate the total energy loss and the energy loss through R_1 are approximately equal. A comparison of the resistive energy losses for charging/discharging rates of 50, 100 and 200 μA is shown in Fig. 10. These differences are significant in terms of optimization of device design for a specific application.

Energy storage efficiencies of 90 and 80% were achieved for final cycles at the 200 and 50 μA rates, respectively.

3.3. Relaxation of charge distribution within the network on open-circuit after charge or discharge

In previous work [14] we have studied open-circuit self-discharge due to one or more mechanisms involving leakage currents. Of equal or greater interest is that an opposite effect of *voltage recovery* takes place when a discharging current is interrupted [15]. This can only be accounted for in the case of a porous electrode, by time-dependent *internal redistribution of charge* within the pore structure at its interfaces (the double-layers).

In the present work, we have examined both open-circuit self-discharge and voltage recovery. Fig. 11a and b show the variations with time of the open-circuit voltages that follow interruption of charging and discharging currents recorded after 7 1/2 complete charge/discharge cycles from 0 to 9.5 V, in the case of self-discharge from 9.5 V; and from zero V in the case of voltage recovery following current interruption after 7 cycles over the same range. The internal redistribution of charge is obvious in the open-circuit self-discharge voltage profiles of Fig. 11a where V_a declines, while V_b has both a recovery and decline and V_c, V_d and V_e show recovery. All voltages approach a common value after sufficient time, that is, about 100 s.

Fig. 11b shows the V vs. t plot that arises following discharge and is opposite in behaviour to that following charging. V_a recovers while V_c, V_d and V_e decline and the potential at V_b shows both decline (initially, like at C_c, C_d or C_e) followed later by recovery (like that at C_a). Again voltages approach a common value after sufficient time, about 100 s, as expected.

These effects must arise by internal flows of charge between the capacitor elements over time-scales determined by the capacitances of the *C*-elements and the resistors. As self-discharge/recovery processes arise due to 'redistribution' of charge among the individual capacitors of the network, they are dependent on the state of charge of each capacitor. Consequently, the self-discharge/recovery behaviour will depend on the 'history' of charge/discharge and will also exhibit a memory effect. Both charge/discharge rate, and the potential range over which the RC network is operated, will influence the self-discharge/recovery phenomena.

While the internal redistributions of charge in pores of a real porous-electrode capacitor device cannot be followed

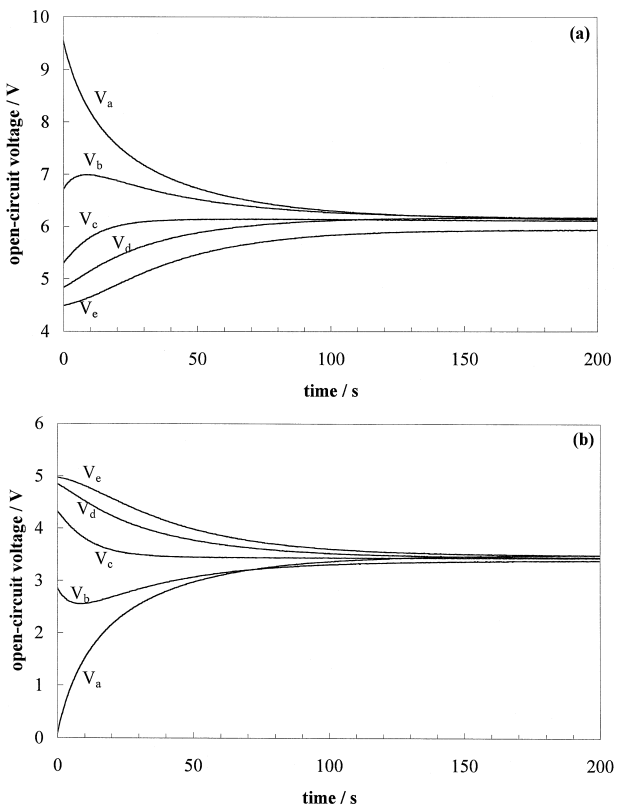

Fig. 11. Voltage/time dependence of the five capacitative elements of the hardware pore-circuit following: (a) External charging at 50 μA to 9.5 V at C_a. (b) Discharging at 50 μA to 0 V at C_a.

experimentally, our previous results in Ref. [14] and results at a gold brush electrode clearly show that complementary overall self-discharge and voltage recovery takes place after termination of charging or discharging, respectively.

With the C and R values used in the hardware network, the relaxation times are in the order of 100 s in either direction. Such times are of the same order as those we have observed [14] in real supercapacitor materials. It is clear, therefore, that these effects will be practically significant especially for the pulsed-charging regimes that are employed in hybrid electric vehicle operation. This relaxation behaviour will depend substantially on the magnitudes of the resistances within the pore network which, for real devices, will be determined by the resistivity of the electrolyte within the pores, the pore lengths and their average diameters. Further work on this aspect is in progress.

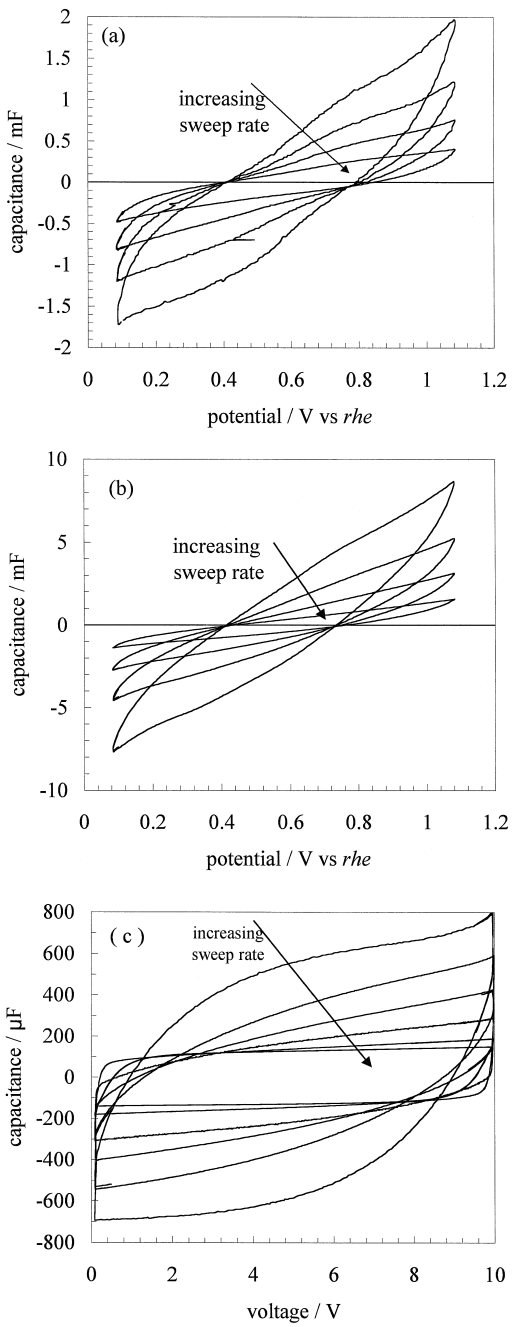

Fig. 12. Capacitance determined from cyclic voltammetry experiments at various sweep rates for: (a) Gold brush electrode in 0.02 M H_2SO_4, (50, 20, 10, 5 mV s^{-1}) (b) Gold brush electrode in 0.2 M H_2SO_4, (50, 20, 10, 5 mV s^{-1}) (c) RC network shown in Fig. 1 (5, 1, 0.2, 0,1, 0.05 and 0.02 V s^{-1}.

3.4. Gold brush electrode

A gold brush electrode can also be used to simulate the electrochemical response of a porous electrode [13]. By operating within the limits of the double-layer region on gold, it is possible therefore to consider and study double-layer charging effects in the absence of any redox complications that may arise at a high-area carbon electrode. It is expected that the double-layer capacitance of a porous electrode (and also a gold brush electrode) determined from CV studies would show a dependence on sweep rate. This is due to the fact that at high rate, the measured capacitance is simply that of the pore orifice, and it is only as the sweep rate slows can the signal penetrate into the pore, thus giving rise to increased measured capacitance. Furthermore, the capacitance at low rate will also deviate from the classical square waveform expected for a pure capacitor due to resistance effects along the pore. Such behaviour was observed for both a gold brush electrode in 0.02 M and 0.2 M H_2SO_4 (Fig. 12a and b) and for the RC network model circuit shown in Fig. 1 (see Fig. 12c). At all sweep rates studied the capacitance of the brush electrode in the 0.2 M acid solution was greater than that in the 0.02 M solution. This can be accounted for by the larger conductivity of the electrolyte contributing to greater penetration of the voltage/current signals.

4. Conclusions

As a result of the simulation experiments described in this paper, several important observations can be made in context of the use of double-layer capacitors in EV-hybrid devices. Porous electrodes are characterized by a 'memory effect' and require some cycling (conditioning) before a 'steady-state' charge/discharge behaviour is achieved. The final state of the device is dependent both on the charge/discharge rate and also on the device design, including factors contributing to device resistances such as choice and concentration of the electrolyte, pore size, shape and distribution. The penetration depth and amplitude of the charge/discharge signal experienced by inner capacitors is dependent on the pore resistance. A conductive electrolyte or less resistive pore will result in both a greater penetration depth and also in charge/discharge

signals of greater amplitude across inner capacitor elements. As a result, the latter are able to accept more charge, at a particular rate, and therefore, the energy storage capacity of the device increases.

Further, choice of carbon material (based on porosity, pore size and pore size distribution) for the double-layer capacitor device is dictated by the application requirements. A careful analysis of requirements is needed, as a complex relation exists between energy storage efficiency, charge/discharge rate, power-density and energy-density. For a given material of certain pore size and distribution, power losses through internal resistances are highest for high-rate charge/discharge, whereas the energy losses are greater at low-rate charge/discharge. This is further complicated, as the energy-density of the porous material increases as the charge/discharge rate decreases.

A practical porous electrode device, modelled as many pores in parallel, will have an overall electrode ESR defined by:

$$\frac{1}{\mathrm{ESR}} = \sum_{i=1}^{n} \frac{1}{R_{\mathrm{p}i}} \approx \frac{n}{R_{\mathrm{p}}} \quad or \quad \mathrm{ESR} = \frac{R_{\mathrm{p}}}{n} \tag{4}$$

(where $R_{\mathrm{p}i}$ is the resistance of the ith pore, and $R_{\mathrm{p}i} \approx R_{\mathrm{p}}$, the average pore resistance).

The overall ESR of the device may be quite small, but the individual pore resistances in any one pore may still be quite large. This point is of significance in terms of the 'penetration depth' of the charge/discharge signal, the non-uniformity of charging and the losses associated with energy and power dissipation through the resistive elements of the circuit.

The extent and rate of self-discharge is another factor to be considered in the design of a double-layer capacitor for a particular application. Self-discharge due to internal redistribution of charge is dependent on the cycle history of the device, and under certain circumstances can lead to relatively fast discharge of a significant portion of the device's capacity.

Acknowledgements

Grateful acknowledgment is made to the Natural Sciences and Engineering Research Council of Canada for support of this work on a Strategic Grant.

References

[1] D.C. Grahame, Chem. Rev. 47 (1947) 441.
[2] K. Kinoshita, Carbon-Electrochemical and Physicochemical Properties, Wiley, New York, 1988.
[3] B.E. Conway, Electrochemical Supercapacitors: Scientific Principles and Technological Applications, Plenum, New York, 1999, in press.
[4] B.E. Conway, V. Birss, J. Wojtowicz, J. Power Sources 66 (1997) 1.
[5] B.E. Conway, in.: F.M. Delnick, M. Tomkiewicz (Ed.), Proc. Electrochem. Soc. Symposium on Electrochemical Capacitors, The Electrochemical Society, Pennington, NJ, 95–29, 1996, 15.
[6] S. Hadzi-Jordanov, H. Angerstein-Kozlowska, B.E. Conway, J. Electroanal. Chem. 60 (1975) 359.
[7] T.C. Liu, W.G. Pell, B.E. Conway, S.R. Roberson, J. Electrochem. Soc. 145 (1998) 1882.
[8] B.E. Conway, in: S. Wolsky, N. Marincic (Eds.), 1st International Seminar on Electrochemical Capacitors and Similar Energy Storage Devices, Florida Educational Seminars, Boca Raton, FL, 1991.
[9] W.G. Pell, B.E. Conway, J. Power Sources 63 (1996) 255.
[10] R. de Levie, Electrochim. Acta 8 (1963) 751.
[11] H. Keiser, K.D. Beccu, M.A. Gutjahr, Electrochim. Acta 21 (1976) 539.
[12] J. Miller, in: S. Wolsky, N. Marincic (Eds.), 4th International Seminar on Electrochemical Capacitors and Similar Energy Storage Devices, Florida Educational Seminars, Boca Raton, FL, 1994.
[13] R. de Levie, Electrochim. Acta 9 (1964) 1231.
[14] B.E. Conway, W.G. Pell, T.C. Liu, J. Power Sources 65 (1997) 53.
[15] T.C. Liu, W.G. Pell, B.E. Conway, Electrochim. Acta 42 (1997) 3541.